Journal of Electroceramics, 7, 197–210, 2001
© 2002 Kluwer Academic Publishers. Manufactured in The Netherlands.

Novel Piezoelectric-Based Power Supply for Driving Piezoelectric Actuators Designed for Active Vibration Damping Applications

ALFREDO VÁZQUEZ CARAZO[1,2] & KENJI UCHINO[1]

[1]*International Center for Actuators and Transducers, Materials Research Institute, The Pennsylvania State University, University Park, PA 16802, USA*

[2]*Department of Research and Development Engineering, Face Electronics, LC, 427 W. 35th Street, Norfolk, Virginia 23508, USA*

Submitted March 13, 2001; Revised October 18, 2001; Accepted October 29, 2001

Abstract. This paper describes a novel step-up DC-AC piezoelectric-based power supply for driving piezoelectric actuators. Piezoelectric actuators have been demonstrated to be very attractive in applications requiring fast response and high actuation force, such as active damping applications. These actuators are commonly installed in self-powered systems (cars, helicopters, aircrafts, satellites, etc.) with limitation in the battery performance, dimensions and maximum weight. Nevertheless, the required driving electrical AC voltage for these actuators is typically in the range of 100 V to 1000 V, quite far from the 9 to 24 V of common batteries. Thus, the use of heavy, large and EMI-noisy electromagnetic transformers becomes necessary which is a drawback for the compact size required. This paper introduces an alternative system for driving piezoelectric actuators using a novel design of piezoelectric transformer, the Transoner®. The proposed solution allows a reduction in size, weight and magnetic noise generation compared to the classical electromagnetic-based systems. The work represents a completely novel approach to the possibilities of piezoelectric transformers for powering high voltage piezoelectric actuators. The solution offers significant advantages in environments requiring high integration, low weight, and low electromagnetic interferences operated with batteries. A circuit configuration capable of converting a 24 V DC input voltage up to 600 V_{pp} AC output voltage with frequency and magnitude control is implemented. Experimental results are presented for a standard multilayer piezoelectric actuator driven at 100 V_{pp} within the range of 10 Hz to 500 Hz.

Keywords: piezoelectric transformer, Transoner®, piezoelectric actuator, piezoelectric converter, active vibration systems

1. Introduction

Two basic techniques have been developed within the prior art in order to damp the noise and vibrations in aircraft and space applications: passive and active attenuation systems (Fig. 1). Passive vibration reduction systems have proved to be successful in the past and they are still widely used in many applications. However, recent reductions in the cost and size of digital computers, and advances in control system technology, have made active vibration systems viable.

Passive attenuation systems include passive blankets, passive Tuned Vibration Absorbers (TVAs) and adaptative TVAs [1, 2]. In these systems, barrier absorbent materials in the fuselages are used to damp the vibrations from the main gear rotor to the cabin. Barrier materials must be relatively dense to be effective in absorbing mechanical vibrations. The higher the density of the material the greater the weight. Thus, the addition of weight to the fuselage of an aircraft to enhance vibration absorption has the adverse effect of reducing fuel economy, payload, and flight range. Passive systems are relatively simple, they have no direct power supply requirements and they have good stability. However, they are only effective for a particular frequency or for a very narrow range of frequencies. Thus, they tend to be characterized by a lack of adaptability with respect to changes in flight conditions, rotor rotational frequency and changes in structural dynamics (due to cargo, fuel and passenger changes), and this is a particularly severe

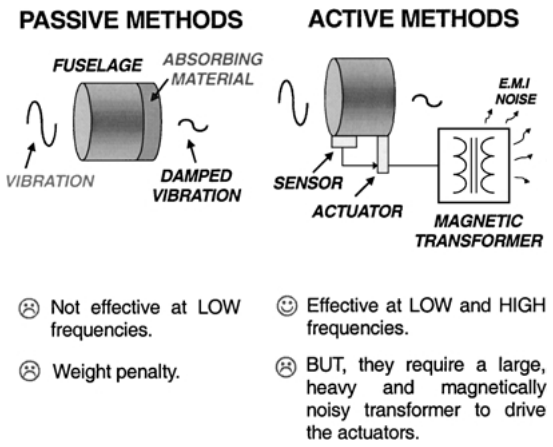

Fig. 1. Passive and active damping systems.

limitation. In addition, passive dampers are effective in attenuating high frequency noise and vibration but they must be very massive if low frequency signals have to be eliminated.

In applications where a higher level of vibration attenuation is desired, active vibration systems [3–7] provide alternative means of controlling the disturbances within the aircraft's cabin. Active systems offer the potential to meet increasingly stringent comfort requirements over significant areas of the aircraft structure. In principle, active vibration systems include actuators to provide the active control forces for isolating vibration. Known active systems include reference signals, such as from accelerometers or vibration sensors, to provide a reference signal of the vibrations of engines. A controller processes the reference signals to generate drive signals of the appropriate phase and magnitude (anti-vibration) to reduce vibration transmission.

Piezoelectric actuators have been demonstrated to be a reliable solution for active damping applications due to their fast response and high actuation force [8, 9]. Particularly, this type of actuator has been considered in helicopter applications for reducing the vibrational noise and enhancing the comfort of the pilot and performance of the devices located in the cabin. However, two important issues [10, 11] in using piezoelectric actuators for active control are: (1) the high electric voltage and significant power required for these devices, and (2) the complexities involved with active control (added hardware, control law design, and implementation). In this paper we describe a novel solution for the first issue.

Solid State Actuators made with piezoelectric materials have evolved greatly in the last decade. Piezoelectric actuators include multilayer actuators, unimorphs, bimorphs, multimorph actuators, MOONIES, CYMBALL, RAINBOW, CRESCENT, and THUNDER® [9, 12]. We have chosen a standard multilayer actuator for implementing the proposed converter, but the solution is extended to all existing actuator technologies.

Typically, piezoelectric actuators require an AC driving electrical voltage in the range of 100 $V_{\max}$ (low voltage actuators) to 1000 $V_{\max}$ (high voltage actuators) [9]. Nevertheless, the battery level in helicopters and other similar self-powered systems is set in the range of 24 V DC. Thus, step-up conversion is necessary in order to drive the piezoelectric actuator. This task is typically made with heavy, large, and electromagnetically noisy electromagnetic transformers. This represents a serious drawback for the general performance of the helicopters. Thus, an objective in the existing active damping systems for helicopter and aircraft applications is focused on replacing the conventional magnetic transformer for a lighter, smaller and electromagnetically compatible device.

A very promising alternative to the electromagnetic transformer for compact, light, no electromagnetic noise, non-flammable, and high efficiency demanding applications is the piezoelectric transformer (PT). C.A. Rosen described the first piezoelectric transformer, PT, in 1956 [13, 14]. Since then, PTs have been successfully applied in high voltage applications, such as inverters to light up the cold cathode fluorescent lamps (CCFL) for backlighting the color liquid crystal displays (LCD) in laptop computers applications [15], with typical equivalent impedance of 100 kΩ or more. However, under such conditions the power capabilities of this PT is very low, around 5 to 10 W, with power densities limited to 5 W/cm^3. This low power capability makes these transformers useless for power conversion applications. Thus, a new PT with high power transfer performance is required for power converter applications. A novel concept of PTs, Transoner® [16, 17], has recently been proposed by Face Electronics, LC, Virginia, USA, for achieving high power transfer demands. Consequently, Transoners are particularly well adapted to power converter applications requiring high power densities, small size, low weight, isolation between primary and secondary and low electromagnetic interferences. Currently, Transoners are manufactured to achieve power levels up to 110 W and power densities

higher than 40 W/cm^3. A sample of Transoner has been successfully used in this application.

The authors propose a novel DC-AC converter using a piezoelectric transformer for driving piezoelectric actuators. The piezoelectric-based converter consists of three main blocks: (i) a resonant inverter which converts the battery DC voltage into an AC voltage; (ii) a high power piezoelectric transformer driven at AC resonant voltage which amplifies the AC output voltage regarding to the input one; (iii) a half-bridge PWM inverter which generates the driving actuator signal through an inductive filter. The proposed system is implemented and the experimental results are shown.

2. Design Considerations

2.1. Spectrum of the Vibrations in a Helicopter

The blades of a helicopter are subjected to periodic alternating forces. These forces cause stresses and reactions in the hub of the rotor and significant bending and torsional moments applied to the shaft of the rotor. These alternating stresses are repeated regularly on each revolution of the rotor and induce, essentially, horizontal and vertical vibrations which propagate through the fuselage. Particularly, these vibrations are very substantial in the cockpit of the aircraft. The vibrations thus generated represent an important drawback in helicopter applications since they can: (i) limit the maximum speed of the aircraft, (ii) weaken its structural strength, (iii) impair the comfort of the occupants of the aircraft and (iv) significantly affect essential control devices for safe navigation, such as the automatic pilot or the helicopter electrical or nocturnal flight control.

In forward flight, the rotor blade experiences asymmetrical loading during each revolution and due to these oscillatory air loads the blade response is rich in harmonic content. In transferring from the rotating frame to the fixed fuselage frame most of the forces and moments generated at the rotor head cancel, while the remainder coalesce into the blade passing frequency, $n\omega$ (where n is the number of blades and ω is the rotational speed of the rotor). Consequently, the fuselage vibration spectrum is dominated by the blade passing frequency $n\omega$, its harmonics, and subharmonics. Typically, the targeted vibrations have the fundamental frequency between 50–100 Hz, with the next higher modes ranging up to 400–600 Hz [10, 18]. In this work we consider an actuation spectrum between 10 Hz up to 500 Hz.

2.2. Actuator Power Requirements

A critical issue that arises when using piezoelectric actuators is the electric power consumption necessary to drive them. Applications are found to depend upon the electrical characteristics of the PZT transducers, namely the capacitive and resistive behavior of the actuator, which in turn affect their power consumption characteristics. When operated far below the resonant frequency a piezoelectric actuator behaves as a capacitive load. This is the case of the present application since the majority of helicopter vibrations occur at low frequency away from the resonance range of the actuator. In such conditions, the displacement generated in the actuator is, in a first approximation, proportional to the electric charge. An equivalent circuit of the piezoelectric actuator is shown in Fig. 2, where the parallel resistance represents the dielectric losses of the actuator. Dielectric losses can be estimated through the dielectric dissipation factor of the actuator, $tg\varphi$ [19], defined as the tangent of the loss angle (the ratio of the parallel resistance to the parallel reactance). Typically, the dissipation factor is in the range of 0.2 to 0.5%. Thus, the actuator basically behaves, in a first approximation, as a reactive load.

Another aspect to consider in the evaluation of the power consumption of the piezoelectric actuator is the dependence of its capacitance on the electrical and mechanical conditions. A number of researchers have investigated the power consumption characteristics of PZT actuators used for active damping. Research by

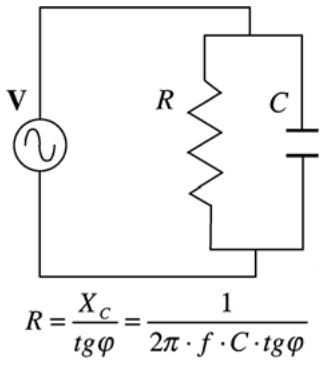

Fig. 2. Equivalent circuit for a piezoelectric actuator operating off-resonance.

Brennan and McGowan [20] shows that the power consumption of piezoelectric materials used for active vibration control is independent of the mechanical motion of the host structure when the structure is completely controlled. From these findings, they conclude that the power requirements of the piezoelectric actuator are only dependent upon its geometry, material properties, and the driving voltage and frequency of the control signal. Nevertheless, they also note a linear variation of the capacitance of the actuator with the applied field, which can be important to avoid large errors in predicting power requirements. Jordan et al. analyzed these non-linearities for PZT-5A based-actuators in reference [21]. In this paper, we will estimate the reactive power required for the actuator. A more extensive analysis including active power (mechanical power and losses in the actuator and the switching amplifier) is postponed for a future work.

In order to estimate the reactive power required, we assume that the actuator is driven with a unipolar sinusoidal wave. This is a general practice to limit the risk of depolarization and also to reduce the fatigue of the actuator. Voltage, current and reactive power in the actuator are obtained in Eqs. (1) to (4):

$$v(t) = \frac{V_{pp}}{2}[1 - \cos(2\pi \cdot f \cdot t)] \tag{1}$$

$$i(t) = V_{pp} \cdot C \cdot \pi \cdot f \cdot \sin(2\pi \cdot f \cdot t) \tag{2}$$

$$p(t) = v(t) \cdot i(t) = \frac{V_{pp}^2}{2} \cdot C \cdot \pi \cdot f \cdot [\sin(2\pi \cdot f \cdot t) - \sin(2\pi \cdot f \cdot t) \cdot \cos(2\pi \cdot f \cdot t)] \tag{3}$$

$$P_{\text{avg}} = \frac{1}{T}\int_0^T v(t) \cdot i(t) \cdot dt = V_{pp}^2 \cdot C \cdot f \tag{4}$$

where $v(t)$, $i(t)$ and $p(t)$ are the time-domain expressions for the current, voltage and instantaneous reactive power in the actuator, V_{pp} is the voltage peak to peak and can be estimated as the DC voltage switched by the amplifier, C is the equivalent capacitance of the actuator (Fig. 2) and f is the frequency of the driving actuator signal. P_{avg} is the average reactive power, related to the steady-state conditions of charging/discharging the actuator.

2.3. Actuator Control and Driving Circuit

Space and aircraft applications have only a little space available. This limitation requires integrated amplifiers with a small number of external components and low power dissipation. Traditional linear amplifiers (classes A, B, C) have been used so far for driving piezoelectric actuators [22]. These amplifiers operate below saturation and have low efficiency, high power consumption, and high power dissipation (needed for heat removal). The previous drawbacks limited the maximum possible efficiency to 78.5% in class-B push-pull amplifiers for a sine wave. In practice the actual efficiency of linear amplifiers dropped typically up to 65% [23] for sine wave and is much lower (15–20%) for real reference signals [24]. Switching amplifiers have appeared recently as an alternative to linear amplifiers in applications where high efficiency and lower consumption are required [23–25]. The theoretical maximum efficiency for all types of switching amplifiers is 100% at all outputs. This fact makes these amplifiers attractive for applications requiring high efficiency and reduced dimensions. The actual efficiency of these amplifiers in practice is reduced typically to 85% for class D, E, or F amplifiers [23]. Recently, class-D amplifiers have been successfully considered in active damping applications and other applications involving piezoelectric actuator control [26–29].

The main idea behind the class-D [30] concept is the conversion of a reference signal (vibration signal, audio signal, etc.) into a pulse width modulated signal (PWM signal) with constant frequency. Since PWM signals have only two levels, a simple switched mode amplifier can be used to obtain high output power. It is well known that the high power efficiency is due to the switched mode operation of the MOSFET switches. The PWM signal must be demodulated in order to reconstruct the (amplified) reference signal. Usually a low pass filter is used for this purpose. The structure of a class-D amplifier is shown in Fig. 3.

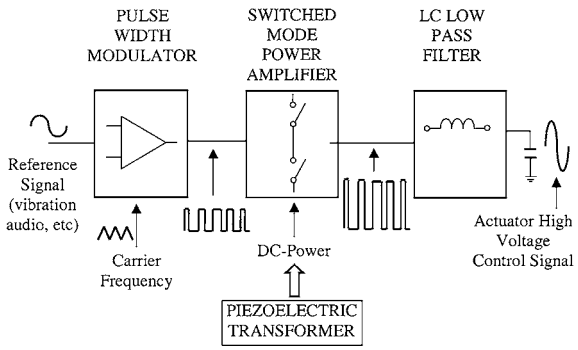

Fig. 3. Structure of a class-D amplifier.

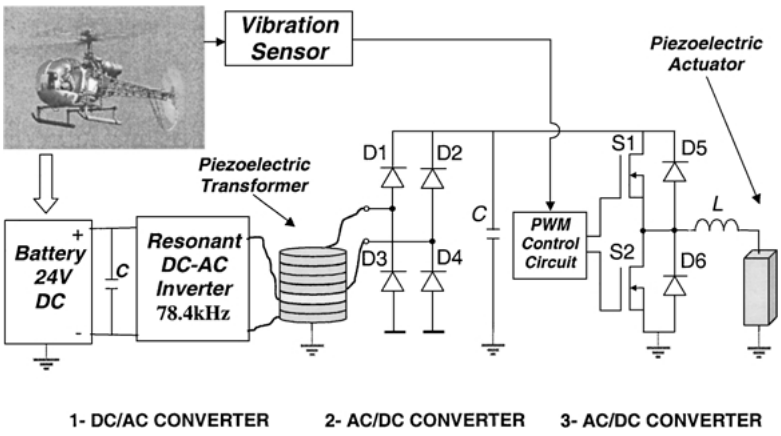

Fig. 4. Piezoelectric-based power converter driving a piezoelectric actuator.

3. Operating Principle of the Proposed System

The developed piezoelectric power supply consists of three power conversion stages, as is schematically shown in Fig. 4. For the particular approach considered in this paper, we assume that the input main power supply is a 24 V DC battery of the helicopter. Similar analysis can be extended to different battery levels and different applications.

3.1. First Stage: DC to AC Inverter for Driving the Piezoelectric Transformer

The battery voltage is led to a first resonant inverter which generates the driving input of the PT. The frequency of the resonant inverter is selected to excite the first mechanical resonance of the PT. Under this condition, the piezoelectric transformer vibrates in its fundamental radial mode and produces a large AC output voltage. Due to the high quality factor, Q, of the PT the output voltage is completely sinusoidal with the same frequency as the PT's input voltage.

3.2. Second Stage: AC to DC Rectifier

The output voltage from the piezoelectric transformer is rectified by using a single-phase diode bridge rectifier and filtered through an electrolytic capacitor in order to obtain a DC voltage. Since the power supply has to be kept relatively stable, the capacitor, C, is selected to be at least 10 times the piezoelectric actuator capacitance. In addition, it is necessary to guarantee that the piezoelectric transformer will deliver a constant output voltage independently of the load condition. This is achieved using a feedback frequency tracking circuit between the input and output of the piezoelectric transformer which maintains the voltage constant. A more detailed description on feedback techniques for piezoelectric transformer operating in DC/DC converter can be found in reference [31].

3.3. Third Stage: DC to AC Inverter with Frequency and Magnitude Control

The resultant DC voltage from the rectifier is switched by the half-bridge amplifier to drive the actuator. As shown in Fig. 4, the rectifier converts into a DC voltage the AC output voltage from the piezoelectric transformer, and the inverter converts DC into adjustable-magnitude, adjustable frequency AC signal. The filtering capacitor, C, is an energy storage element and actuates as a DC link between the rectifier and the output inverter. Frequency and magnitude actuator control are achieved using PWM technique from a reference input signal from a vibration sensor. The signal arriving to the actuator is finally filtered through an inductance, which eliminates the high frequency components used for the PWM switching.

Figure 5 summarizes the proposed system applied to helicopter vibration damping. A piezoelectric actuator is used as an active vibration device. Vibration sensors can be used to detect noise and/or vibration to be controlled within the pilot cabin. Actuators and sensors are electrically connected to the driver/controller. The control system, driver/controller, acts responsive to input

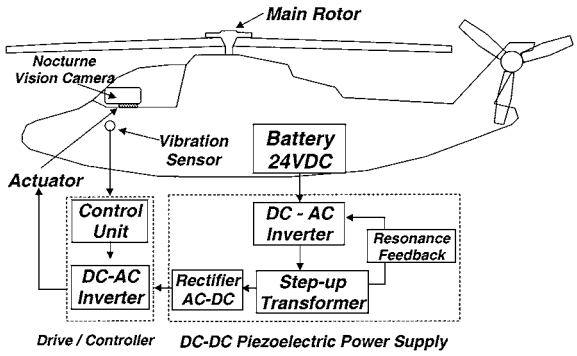

Fig. 5. Particular application of the proposed system in active damping for aircraft.

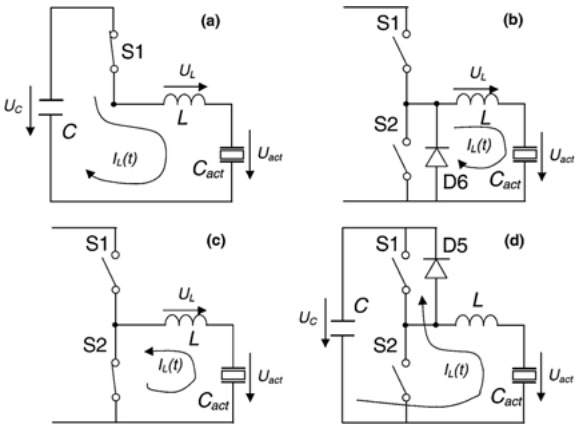

Fig. 6. Operation of the output DC/AC converter.

from the sensor to drive the actuator in a manner to reduce or eliminate noise and/or vibration generated by the vibrational energy sources (engines).

In the operation of the output inverter, Fig. 6, the piezoelectric actuator is charged when the switch S1 is closed and S2 is opened (Fig. 6(a)). A current, $i_L(t)$, is then established through the series circuit formed by the switch S1, the inductance L, and the actuator. This current flow causes energy to be stored in the inductance due to the positive potential difference between the filtering capacitor and the actuator. The reactive energy stored in the filtering capacitor C is then delivered to the actuator. When the charging switch S1 is opened, Fig. 6(b), the current $i_L(t)$ continues flowing through the series circuit formed by the piezoelectric actuator, the inductance L, and the internal diode of the switch S2, diode D6. This energy flow causes all of the energy stored in the inductance to flow into the piezoelectric actuator. Thus, the voltage arising at the piezoelectric actuator (as well as its external dimensions) increase in response to the energy supplied to the actuator. At this point, the discharging switch, S2, is closed and the conditions indicated in Fig. 6(c) arise. A series circuit formed by the actuator, the inductance, and the switch S2 is then formed. Thus, the energy stored in the actuator is transferred to the inductance L and a current $i_L(t)$ is established as indicated in Fig. 6(c). The voltage arising on the actuator, as well as its external dimensions, decreases in response to the energy transfer from the actuator to the inductance. When the discharging switch S2 is then opened, the conditions indicated in Fig. 6(d) appear. In this situation, the energy flow causes the energy stored in the inductance L to flow back into the capacitor. Thus, the energy is exchanged between the power supply and the piezoelectric actuator without, ideally, any losses. The driver circuit needs to be able to charge and discharge the actuator capacitance for all the voltage and frequency operation range. Particularly, switched amplifiers are able to recycle this energy with high efficiency, so that the needed line-power has only to cover the (much smaller) active part of the power balance. This active power is (a) drawn from the system as mechanical power, (b) dissipated by self heating of the actuator due to the dielectric losses, (c) dissipated in the series resistance of the filtering inductance and (d) dissipated in the switches of the amplifiers during the "on" and "off" actuation.

4. Construction

4.1. Piezoelectric Actuator

The $10 \times 10 \times 20\ \text{mm}^3$ multilayer actuator from Tokin Corp. [32], was utilized as actuator for active control. Because the majority of spacecraft vibrations occur at low frequencies, the capacitance and the dielectric dissipation of the actuator were measured from 1 Hz up to the first resonance peak. The NF 5090 Frequency Response Analyzer from NF Electronics Instruments, Japan, was used for measuring the admittance of the sample and thus evaluates the power consumption. A sinusoidal input voltage of 5 V_{pp} was used for the measurements. The admittance and phase curves are shown in Fig. 7. The capacitance measured was 6 μF for the operating range up to 500 Hz.

The maximum required average power is estimated using Eq. (4) and considering the maximum operation

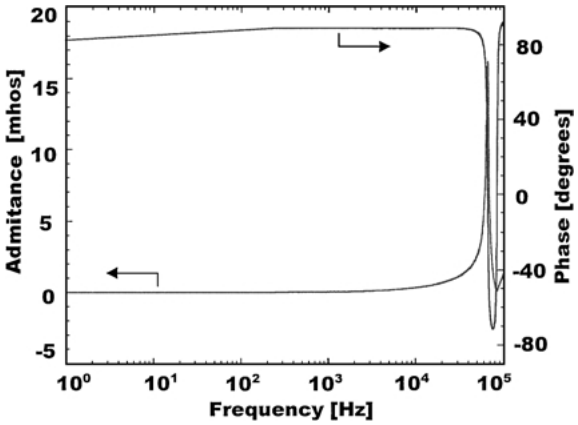

Fig. 7. Admittance and phase spectrum for the stack actuator TOKIN-101016.

voltage and frequency. In our application, the frequency range is extended up to 500 Hz and the input voltage is expected to be up to 100 V_{pp}, and then:

$$P_{\text{avg}} = V_{pp}^2 \cdot C \cdot f = 30\,\text{W} \tag{5}$$

Since an active damping actuator needs to operate in dynamic conditions changing frequently the operation frequency, it is also necessary to estimate the maximum peak power required from the amplifier. This peak power is associated with the peak current required to charge and discharge the actuator in dynamic conditions:

$$P_{\text{max}} = \pi \cdot V_{pp}^2 \cdot C \cdot f = 94.24\,\text{W} \tag{6}$$

In addition to the power consumed by the actuator, the battery needs to supply power to the driving circuitry (gates drivers, PWM function generator circuit, etc). This power, estimated to be less than 750 mW ($\pm$15 VDC under 25 mA), does not play a role in the power transfer through the converter, since it was directly taken from the main supplying battery with an auxiliary linear regulator.

4.2. High Power Piezoelectric Transformer: The Transoner®

Transoner-type PTs differ from Rosen-type transformers in two key aspects: (a) the design and (b) the electromechanical coupling between input and output parts. Transoners are constructed by multilayering single individual disks in the thickness direction. Particularly, the output part consists of several thin layers connected in parallel in order to have low impedance and thus achieve high power transfer characteristics under low or medium loads (1 Ω–10 kΩ range), depending on the selected design. Transoner is the first multilayer transformer developed which uses radial-extensional vibration in the input and output parts. Transoners are typically driving in their first radial-extensional vibration mode. The vibrations under such conditions follow a Bessel function and are dependent on the input and output radial coupling coefficient. Typically, for PZT-based materials, the radial electromechanical coupling coefficient is up to twice as high as the transversal coupling factor k_{31}, typically used in Rosen-type transformers. In addition, the coupling area between the input and output layers is extended to all the surface area in comparison to the smaller transverse area in Rosen-type transformers. This makes larger the so called "force factor" [31] of the transformer, which is a measure of its power capabilities. Therefore, the power transmission of Transoner-type transformers is greatly improved. An additional advantage of Transoner PTs is their simplicity to be designed with input and output isolated from each other, an important requirement in applications involving full-bridge rectifiers (see Fig. 5). Figure 8 shows the isolated Transoner used for this application with 25 mm diameter and a total thickness of 6 mm and power capabilities higher than 70 W.

The NF 5090 Frequency Response Analyzer from NF Electronic Instruments, Japan, was used for measuring the input and output voltages and currents. This equipment has the capability to acquire AC signals up to 200 V. Current was measured by using the AM503B AC/DC current probe amplifier and the A6302 current probe both from Tektronix, Inc., Wilsonville, OR, USA. Input and output voltages were measured with high impedance probe P5100 (10 MΩ, 2.5 pF) from Tektronix. The load effect was characterized by connecting a resistance bridge with a range from 1 kΩ to 10 kΩ. The input driving voltage to the transformer was taken from the oscillator output of the Frequency Analyzer. This output generates sinusoidal AC signals up to $\pm$10 V/$\pm$100 A. The oscillator output was driven through the NF4025 High Speed Power Amplifier, from NF Electronic Instrument, in order to increase the voltage and power range of the input voltage to the sample. The monitored voltage and current were driven through a GPIB connection to a computer for

Fig. 8. Piezoelectric transformer, Transoner®, operating in radial-extensional vibration mode.

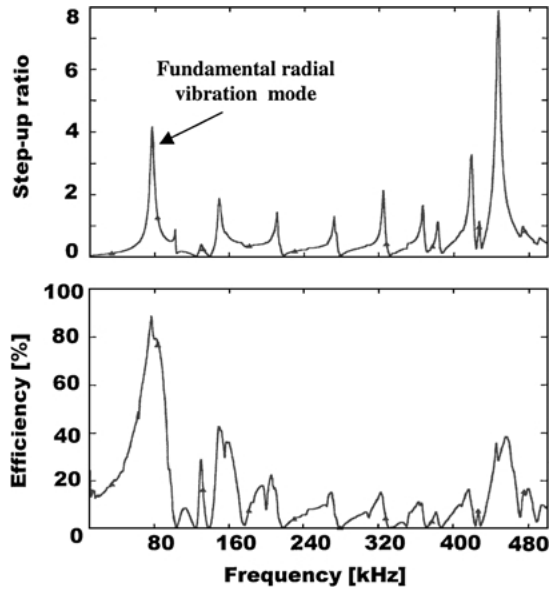

Fig. 9. Efficiency and step-up ratio spectrum (10–500 Hz) for the PT LB2-B Transoner® from Face Electronics.

computing power, efficiency and step-up ratio. Figure 9 shows the efficiency and step-up spectrums of the piezoelectric transformer for a broad spectrum in the range from 10 kHz to 500 kHz. The 1 kΩ resistance was connected as a load in the output of the transformer and 800 measuring points were taken through the NF 5090 Frequency Response Analyzer. Higher step-up ratio was obtained around 470 kHz, nevertheless the efficiency decreased up to 40% with significant heat generation. On the contrary, the first resonance frequency around 78 kHz showed a high efficiency combined with a large step-up ratio.

Figures 10 and 11 illustrate a zoom particularly referring to the first transversal resonance around 78 kHz, showing the efficiency and step-up spectrums for the transformer. A 400 points sweeping voltage of 10 V_p input was applied during the measurements. Different resistive loads were connected in the output of the transformer to evaluate their dependence. Maximum efficiency (Fig. 10) for the first radial resonance was obtained under 1 kΩ load, rising 91%. Under the same conditions, the measured step-up ratio was 2.77, as illustrated in Fig. 11. The step-up ratio increased under higher loads, with decreasing the efficiency.

4.3. Half-Bridge Inverter (Class-D Amplifier)

The complete circuit diagram of the PWM power MOSFET-based amplifier has been depicted in Fig. 4.

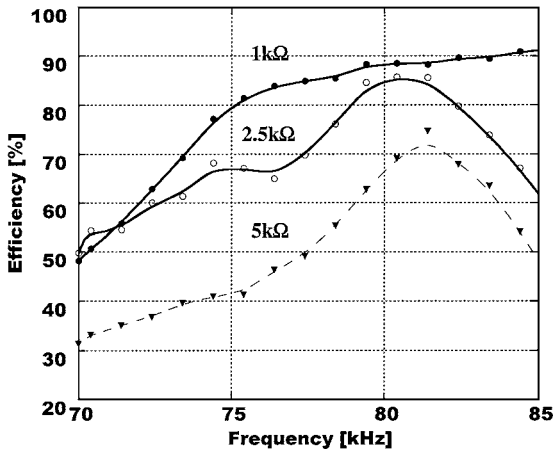

Fig. 10. Efficiency spectrum for the PT LB2-B Transoner® in the first radial mode under different resistive loads.

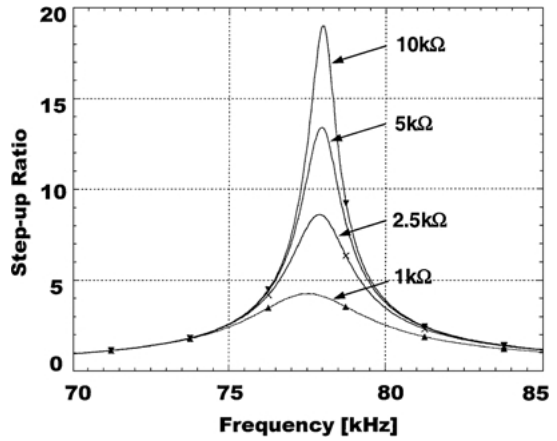

Fig. 11. Step-up ratio spectrum for the PT LB2-B Transoner® in the first radial mode under different resistive loads.

The design is divided into three main parts namely a PWM modulator, a power stage and a LC low pass filter (demodulator).

4.3.1. Pulse width modulator. As shown in Fig. 12, the PWM modulator circuit consists of (1) a triangular waveform, (2) a reference vibration signal, (3) a comparator level sensitive circuit and (4) a high speed Power MOSFET driver. The generation of the PWM waveform is achieved by comparing directly the reference vibration signal with the triangular carrier wave to determine the switching instants and therefore the resultant pulse widths. The *triangular waveform*

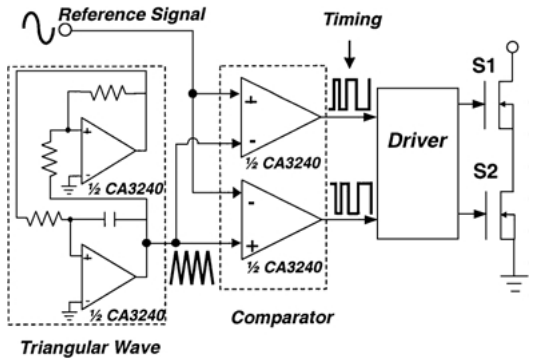

Fig. 12. PWM circuit generator and MOSFET driver.

$(T(t))$ was generated by using two operational amplifiers included in the CA3240 integrated circuit. A ramp generation plus an integrator circuit implemented the waveform. The selected carrier frequency was 40.5 kHz, which is more than 40 times longer than the maximum broadband of the reference signal (<1 kHz). The triangular carrier waveform has a fixed amplitude of 11 V_{pp}.

Vibrational energy (*reference signal*, $M(t)$) is taken directly from a vibration or an acceleration sensor. Depending on the type of sensor used or the magnitude of the signal read, it could be necessary to use a preamplifier or a signal adapter circuit. In general, in the closed loop configuration, the control signal will come from the integration of the error signal from the external control signal and a feedback signal. Nevertheless, in the present study we consider an open-loop topology and the reference signal is taken directly from the sensor. The reference signal (or the error signal, depending on whether the open or closed loop is used) and the carrier signal are fed simultaneously into two *comparators* to generate the PWM pulses. One of the comparators is working as a non-inverter and the other one as an inverter respective to the control signal. This allows to get two complementary PWM signals, one the inverse of the other one. These two timing signals permit the control of the turn on and off of both of the switches of the half-bridge. The two comparators were built in a double operational amplifier chip, CA3240 (Fig. 12). The output timing signals were led to a high and low IR2113 driver from International Rectifier. The IR2113 is a high voltage, high speed Power MOSFET driver with independent high and low side referenced output levels. The gate drive supplies the gate control voltage in the range of 10 to 20 V for turn-on the switches and

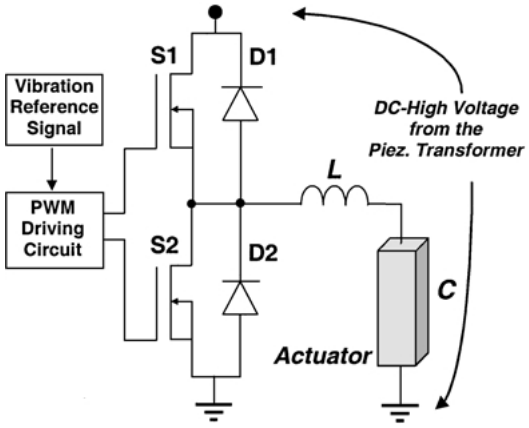

Fig. 13. Power-stage of the implemented Class-D amplifier (Half-Bridge inverter).

permits full voltage switching operation voltage up to 600 V.

4.3.2. Power stage circuit. A prototype of switching amplifier based on the Class-D (half-bridge) configuration has been developed as shown in Fig. 13. The half-bridge inverter has two controlled static switching element, implemented by two n-channel mode HEXFET® Power MOSFET IRPFE50 from International Rectifier, CA, USA. Each switch, labeled as S1 and S2, has an internal built-in anti-parallel diode (D5 and D6 respectively) necessary for the correct operation of the circuit. The two gates of the Power MOSFETs are electrically connected to the driving circuit responsible for generating the timing/control signals. The pulse-width of the pulse-width modulated signal (PWM) within the driver is varied by the driver responsive to control signal from controller circuit to provide in the switching electrical output signal of the FET driver circuit, the frequency signal range of the vibrational energy to be controlled. Actuator is electrically connected to the driver and generates a complementary vibration to the sensed vibration in order to damp it.

4.3.3. Demodulator filter. A low pass filter is used to remove unwanted high frequencies. The filter is designed such that the carrier and its associated harmonics are significantly attenuated without reducing the amplitude of the desired signal component. The cut frequency of the filter can be determined from the

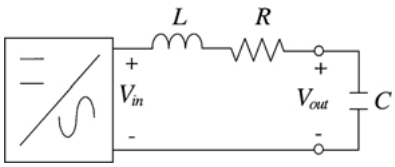

Fig. 14. Demodulating (low-pass LC filter) output circuit.

transfer function of the L-C output circuit due to the filtering inductance L and the serial actuator capacitance C (Fig. 14) as follows:

$$H(j\omega) = \frac{V_{\text{out}}}{V_{\text{in}}} = \frac{\frac{1}{C \cdot L}}{-\omega^2 + j \cdot \omega \cdot \frac{R}{L} + \frac{1}{C \cdot L}} \quad (7)$$

where R is the resistance due to the wire of the inductance. The cut frequency is obtained as:

$$f_0 = \frac{1}{2\pi \cdot \sqrt{C \cdot L}} \quad (8)$$

The output inductor is a key element in the performance of the class-D amplifier system. It is important that these inductors have a high enough current rating and a relatively constant inductance over the frequency range and temperature. The current rating should be higher than the maximum current expected in all the load conditions to avoid magnetically saturating the inductor. When saturation occurs, the inductor loses its functionally and looks like a short circuit to the PWM signal, which increases the harmonic distortion considerably.

In the present application we selected $L = 100$ mH, which guarantee a low frequency pass band of 1290 Hz with an equivalent actuator capacitance of $C = 6\,\mu$F.

5. Experimental Operation of the System

5.1. Experimental Results of the Transformer

In the operation of the complete system (Fig. 5), the first step is to drive the piezoelectric transformer at its first mechanical resonance. A DC-AC ZVS (Zero Voltage Switching) resonant inverter [33, 34] was used to generate the driving input signal of the PT at 78 kHz. The amplitude of the driving switched voltage was selected as 40 V_{pp}, which was considered the bipolar equivalent voltage that should be achieved from a 24 V_{DC} battery.

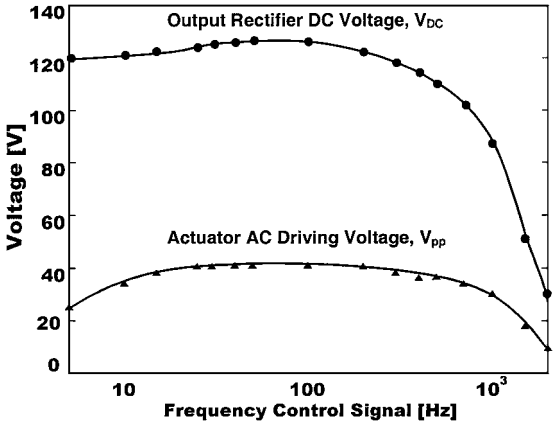

Fig. 15. Input driving voltage to the piezoelectric transformer (78.4 kHz) and output DC voltage after being rectified.

The output signal from the transformer was led to a rectifier and a capacitor filter of 250 V/10 μF, which serves as a power voltage for the amplifier.

Figure 15 shows the input voltage to the piezoelectric transformer and the resultant output voltage after the rectifier. The measurements were taken with the PT driven at 78.4 kHz and 40 V_{pp} input. The rectifier output was connected to the amplifier circuit controlling the actuator in order to verify the behavior of the load in the DC voltage after rectification. A fixed reference signal of 5 V_{pp} (54% modulation index, see Eq. (6)) for a frequency range up to 1.5 kHz was applied to the amplifier. The reference signal was swept by using a Hewlett Packard 33120A Function Generation. The DC voltage generated for the piezoelectric transformer after rectification and the output voltage through the actuator were measured. The output voltage in the piezoelectric transformer, after rectification, was maintained in the range of 120 V for all the control signals up to 800 Hz. When the frequency was increased above this range, the power capabilities were reduced, as expected, and the voltage decreased. Consequently, the driving voltage in the actuator was also affected. The measurements were repeated for different modulation index without appreciable fluctuation in the rectified DC voltage.

5.2. *Experimental Results of the DC-AC Output Converter*

In the operation of the piezoelectric actuator, there is the need to adjust the AC frequency and the AC voltage with regard to the reference signal. Frequency is easily adjusted by variation of the frequency of the clock oscillator of the switching control circuit. This automatically happens if we keep constant the modulating triangular wave, $T(t)$, and the frequency of the reference signal (sensed vibration) is varied. Voltage adjustment can be made by varying the input DC voltage to the inverter by changing the modulation index M, defined as:

$$M = \frac{Amplitude\ of\ reference\ wave}{Amplitude\ of\ carrier} \tag{9}$$

From the previous equation, it is clear that the maximum control signal must be limited to 11 V_{pp} (100% index modulation) for the higher expected vibration. Figure 16 shows the carrier triangular signal used for the PWM control circuit. The amplitude and frequency of the carrier were fixed at 11 V_{pp} and 40.5 kHz, respectively. In the same figure, as a particular example, is illustrated a control signal (modulating signal) of 6 V_{pp} and 1 kHz. The modulation index, in these particular conditions, is 54.5%.

Figure 17 shows the PWM timing signal in the gate of the Power MOSFETs for controlling the ON and OFF states measured in the output of the IR2113 driver integrated circuit (Fig. 11). This PWM voltage is switched between 14 V and 0 V, which guarantee the correct switching of the MOSFETs.

The output current and voltage waveforms in the piezoelectric actuator are indicated in Fig. 18. In

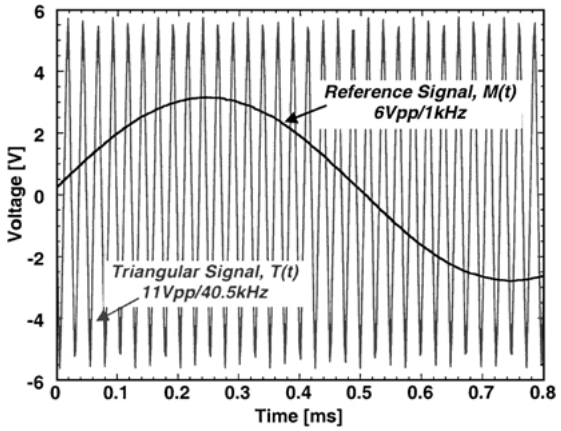

Fig. 16. Carrier (triangular) and reference (vibration) waveforms before the comparator input.

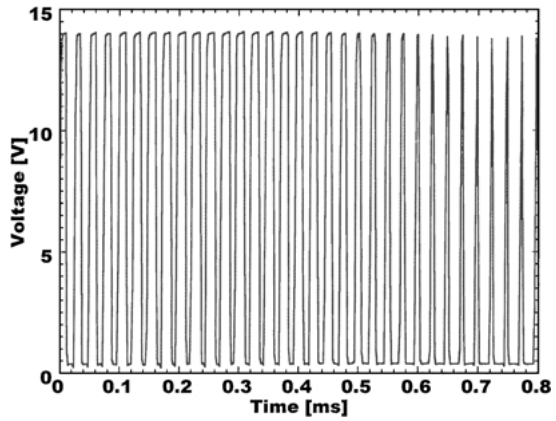

Fig. 17. PWM timing signal for the gate-MOSFET control.

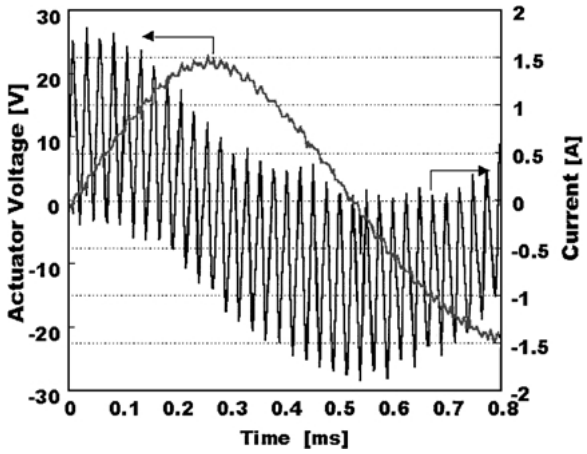

Fig. 18. Output actuator voltage and consumed current after filtering.

this case, the waveforms correspond with a control signal of 5 V_{pp} (54% modulation index) and 1 kHz. The current waveform has the typical triangular shape due to the filtering effect of the 100 mH output inductance and is modulated by the control signal of 1 kHz. The half bridge amplifier and grounded actuator configuration guarantees that the voltage in the actuator is always positive. In Fig. 18, the AC component has been represented. It can be observed how the voltage output is completely sinusoidal as expected due to the filtering effect of the inductance, which removes all the high frequency switching harmonics.

6. Prototype Performance

A general view of the prototype constructed is shown in Fig. 19. The performance of the complete system was analyzed by testing the system at different levels of modulation indexes namely 11, 54 and 74% in the range from 10 to 1000 Hz. The free displacement of the actuator under these conditions was measured using the SDP-2810 Eddy-current displacement sensor from Kaman Measuring Systems and the results are shown in Fig. 20. The curves show how the displacement in the actuator can be varied in frequency and amplitude by modifying the control signal. During the measurements, the input driving voltage in the piezoelectric transformer was maintained as 40 V_{pp}/78.4 kHz being the switching voltage (voltage after the rectifier) 120 VDC.

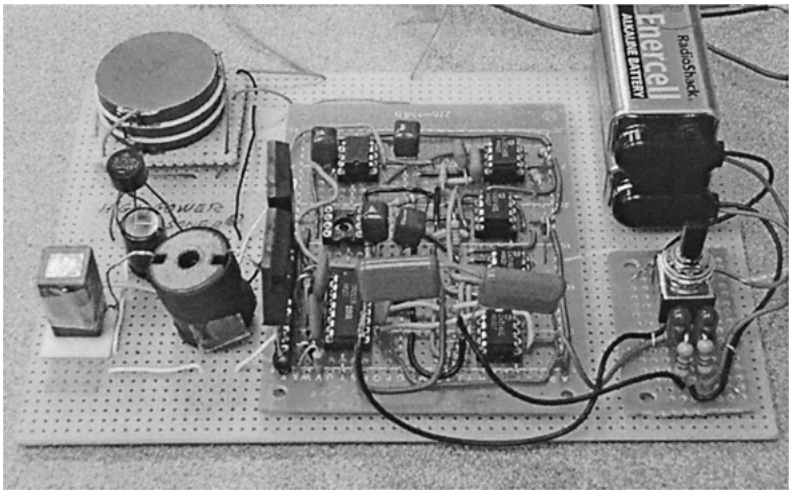

Fig. 19. View of the developed piezoelectric converter driving a multilayer actuator.

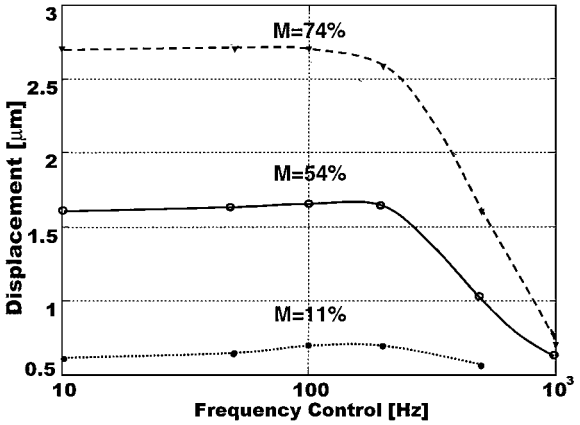

Fig. 20. Displacement control by the modulation index and frequency control.

7. Conclusions

A novel piezoelectric based power supply for driving a piezoelectric actuator was designed, constructed and tested. The piezoelectric converter uses a high power piezoelectric transformer, Transoner, which allow high power transfer. The piezoelectric transformer generates an AC voltage that after rectified was used as the DC high voltage required for the piezoelectric actuator. The magnitude and frequency control of the actuator displacement was controlled from an external vibration signal by switching the DC voltage of the piezoelectric transformer using a class-D amplifier. PWM technique was used for controlling the switching time. The frequency capabilities of the designed system were successfully tested in the range of 10 to 500 Hz, which is the spectrum of the vibration appearing in aircraft and space application, such as helicopter cockpits. The developed system represents the first application using a piezoelectric transformer for driving a piezoelectric actuator. The proposed application field of the system is in battery-powered systems with size and weigh limitations, such as active vibration systems for aircraft applications.

Acknowledgments

The authors would like to thank Mr. Brad Face, Dr. Karla Mossi and Mr. Paul Schmidt, Face Electronics, LC, for the samples of Transoner®.

References

1. R.H. Bennet Jr. and J.D. Van Dyke Jr., U.S. Patent no. 3,490,556, Jan. 20, 1970.
2. H.W. Adams, R.H. Bennet, J.W. Schendel, and J.D. Van Dyke, U.S. Patent no. 3,487,888, Jan. 6, 1970.
3. S.P. King, *Aeronautical Journal*, **92**, 247 (1998).
4. G. Billoud, U.S. Patent no. 5,638,304, Jun. 10, 1997.
5. C.R. Fuller, U.S. Patent no. 4,715,559, Dec. 29, 1987.
6. C.A. Yoerkie Jr., W.A. Weish, and T.W. Sheehy, U.S. Patent no. 5.310.137, May 10, 1994.
7. W.E. Schmidt, D.E. Ivers, M.R. Jolly, and M.A. Norris, U.S. Patent no. 5,906,254, May 25, 1999.
8. K. Uchino, in *Proc. of Intl. Symp. Michromechatronics and Human Science* (1999), p. 3.
9. K. Uchino, *Piezoelectric Actuators and Ultrasonic Motors*, 3rd ed. (Kluwer Academic Publishers, Boston, 2000).
10. J.T. Pearson, R.M. Goodall, and I. Lyndon, *Computing & Control Engineering Journal*, **5**, 277 (1994).
11. A.-M.R. McGowan, in *CEAS/AIAA/ICASE/NASA Langley International Forum on Aeroelasticity and Structural Dynamics*, Jun 01, 1999, p. 553.
12. K. Mossi, G.V. Selby, and R. Bryant, *Materials Letters*, **35**, 39 (1998).
13. C.A. Rosen, in *Proc. Electronic Comp. Symp.* (1956). p. 205.
14. C.A. Rosen, K.A. Fish, and H.C. Rothenberg, U.S. Patent no. 2,830,274, March 7, 1961.
15. S. Kawashima, O. Ohnishi, H. Hakamata, S. Tagami, A. Fukuota, T. Inoue, and S. Hirose, in *Proceedings IEEE International Ultrasonic Symp.*, Vol. 1 (1994), p. 525.
16. R.P. Bishop, U.S. Patent no. 5,834,882, Nov. 10, 1998.
17. R.P. Bishop and C.D. Boyd, U.S. Patent no. 6,052,300, Apr. 18, 2000.
18. W.K. Wilkie, P.H. Mirick, and C.W. Langston, NASA TM-4760, 1997.
19. K. Uchino and S. Hirose, *IEEE Trans. on Ultrasonics, Ferroelectrics and Frequency Control*, **48**, 307 (2001).
20. M.C. Brennan and A.-M.R. McGowan, *Proceedings of SPIE: Smart Structures and Materials*, **3039**, 660 (1997).
21. T. Jordan, Z. Ounaies, J. Tripp, and P. Tcheng, in *Materials Research Society Fall Meeting*, Boston, Massachusetts, 1999.
22. J.W. Wanders, *Piezoelectric Ceramics*, 1st ed. (Philips Components, Eindhoven, The Netherlands, 1991), p. 26.
23. N.O. Sokal, in *Proc. Electron. Ind. Forum of New England* (1997), p. 179.
24. F.H. Raab, *IEEE Trans. Consumer Electron.*, **CE-32**, 145 (1986).
25. N. Mohan, T.M. Undeland, and W.P. Robbins, *Power Electronics: Applications, and Design*, 2nd ed. (John Wiley & Sons, New York, USA, 1995).
26. J. Reineke and A. Hock, U.S. Patent no. 6,081,061, Jun. 27, 2000.
27. D.J. Clingman, *Proceedings of SPIE: Smart Structures and Materials*, **3044**, 459.
28. D.J. Clingman and M. Gamble, *Proceedings of SPIE: Smart Structures and Materials*, **3674**, 280.
29. M.C. Heath, U.S. Patent no. 5,802,184, Sept. 1, 1998.
30. M.K. Kazimierczuk, *IEE Proc. B, Electric Power Appl.,* **6**, 285 (1991).

31. S. Hamamura, D. Kurose, T. Ninomiya, and M. Yamamoto, in *IEEE 7th International Power Electronics Congress Proc.,* Oct. 2000, p. 3.
32. www.tokin.com.
33. H. Tanaka, T. Ninomiya, M. Shoyama, and T. Zaitsu, in *Power Electronics Specialists Conference, PESC 98, 29th in Annual IEEE*, 1998, Vol. 1, p. 655.
34. T. Ninomiya, M. Shoyama, T. Zaitsu, and T. Inoue, in 20*th International Conference on Industrial Electronic Control and Instrumentation, IECON '94*, Sept. 1994, Vol. 3, p. 1665.